

Analysis of Shell Deformation Responses by the Meshless Local Petrov-Galerkin (MLPG) Approach

T. Jarak¹, J. Sorić¹ and J. Hoster¹

Abstract: A meshless computational method based on the local Petrov-Galerkin approach for the analysis of shell structures is presented. A concept of a three dimensional solid, allowing the use of completely 3-D constitutive models, is applied. Discretization is carried out by using both a moving least square approximation and polynomial functions. The exact shell geometry can be described. Thickness locking is eliminated by using a hierarchical quadratic approximation over the thickness. The shear locking phenomena in case of thin structures and the sensitivity to rigid body motions are minimized by applying interpolation functions of sufficiently high order. The numerical efficiency of the derived concept is demonstrated by numerical examples.

Keyword: meshless formulation, shell structures, solid-shell concept, exact shell geometry description, moving least squares interpolation, locking effects.

1 Introduction

In recent years, a new class of numerical approaches known commonly as meshless methods has attracted a considerable attention due to its ability to solve boundary value problems without meshing procedures. Using these new numerical procedures, a computational model, in contrast to the traditional Finite Element Method (FEM), may be discretized only by a set of nodes which do not need to be connected into elements. Therefore, nodes can be easily added or removed without burdensome remeshing of the entire structure. In addition, some difficulties associated with

the FEM such as element distortion and different locking phenomena may be efficiently overcome by using meshless formulations. The order of interpolation functions may be increased without increasing the number of grid points. Thus, some locking phenomena can be efficiently minimized only by increasing the order of interpolation functions with the unchanged number of unknown variables, which is an advantage in comparison with finite element formulations, especially when shell structures are analyzed.

Most of available meshless formulations for shell analysis [Krystl and Belytschko (1996); Noguchi, Kawashima and Miyamura (2000); Kim, Choi, Chen and Botkin (2002); Liu (2003); Chen and Wang (2006)] employ either the Kirchhoff or Mindlin-Reissner type kinematics. It is well known that these formulations are not appropriate for the application of general 3-D constitutive laws, which are usually necessary for the modelling of shell deformation responses, especially when material nonlinearities are considered. Furthermore, the shell geometry generally is described approximately. It is also to be noted that these formulations are not truly meshless because they require a background mesh for numerical integration. A meshfree thin shell formulation based on an extrinsic enrichment has been proposed by Rabczuk and Areias (2006). Herein, an extrinsic basis to increase the order of approximation completeness is used. Like in the formulations mentioned above, integration of global governing equations has been performed over background cells too.

In the present contribution, the Meshless Local Petrov-Galerkin (MLPG) Method, originally proposed by Atluri and Zhu (1998), is applied to the analysis of shell structures. This novel nu-

¹ Faculty of Mechanical Engineering and Naval Architecture, University of Zagreb, Ivana Lučića 5, 10000 Zagreb, Croatia.

merical approach requires no elements or background cells in either interpolation or integration and therefore belongs to truly meshless methods. In addition, the exact shell geometry description can be performed. Discretization of the shell continuum is carried out by sets of nodes located on the upper and lower shell surfaces. A Local Symmetric Weak Form (LSWF) of governing equations over a local sub-domain surrounding a couple of nodes on the shell surfaces is derived. Quadratic test function is employed and essential boundary conditions are enforced by using a penalty method. The proposed formulation is based on the solid-shell concept, allowing the use of complete 3-D constitutive models.

Analogous to the finite element formulation available in the literature such as in Tan and Vu-Quoc (2005), Klinkel, Gruttmann and Wagner (2005) and in the references therein, approximation of displacement field is performed separately in the transversal and in the in-plane directions. Simple polynomial functions are utilized in the transversal direction, while the Moving Least Square (MLS) approach is employed to approximate the displacement components in the in-plane directions. The unknown variables are three fictitious displacement components associated with the nodes located on the lower and upper shell surfaces as well as additional scalar variables due to the quadratic interpolation of the transversal displacement in the thickness direction. Quadratic interpolation is needed in order to avoid undesired thickness locking. Because of additional scalar variables, additional equations for the solution of boundary value problem are required. According to the meshless formulation for plate analysis in [Sorić Li, Jarak and Atluri (2004); Li, Sorić Jarak and Atluri (2005)], an approach with the hierarchical quadratic interpolation over the thickness is adopted.

In contrast to the formulation in Sorić Li, Jarak and Atluri (2004), where a closed system of equations is obtained by enforcing additional equilibrium conditions, in this contribution additional equations are derived by using the quadratic test function through the shell thickness. Thus, the complex second derivatives of the shape func-

tions are avoided, which improves numerical efficiency. Furthermore, shear locking in the case of thin shells and sensitivity to rigid body motions due to the exact geometry description are minimized by applying a sufficiently high order of the basis functions in the MLS approximation. This straightforward procedure can be performed without adding additional nodes to the original computational model. The numerical efficiency of the proposed meshless computational method is finally demonstrated by numerical examples.

2 Geometry description of shell structures

According to the solid shell concept, the geometry of the shell continuum may be described in the global Cartesian coordinates by

$$\begin{aligned} \mathbf{X}(\theta^j) &= X^i \mathbf{e}_i \\ &= \frac{1}{2} \left(1 + \frac{2}{h} \theta^3 \right) \mathbf{X}_u(\theta^\alpha) + \frac{1}{2} \left(1 - \frac{2}{h} \theta^3 \right) \mathbf{X}_l(\theta^\alpha) \end{aligned} \quad (1)$$

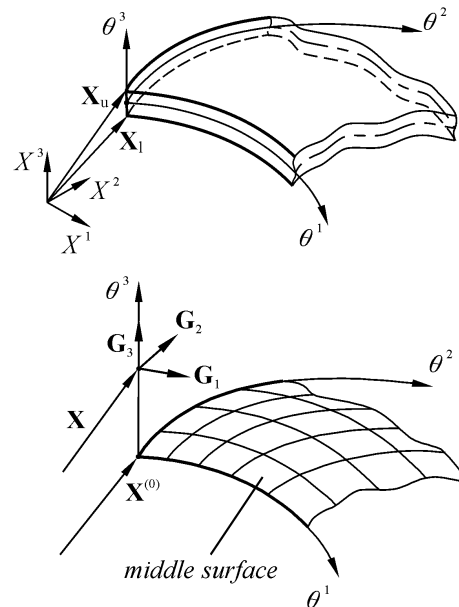


Figure 1: Geometry description of shell continuum

as shown in Figure 1, where $\mathbf{X}_u(\theta^\alpha)$ and $\mathbf{X}_l(\theta^\alpha)$ are the upper and lower surface position vectors,

respectively. Relation (1) may be rewritten in a form more convenient for shell analysis as

$$\mathbf{X}(\theta^j) = \mathbf{X}^{(0)}(\theta^\alpha) + \theta^3 \mathbf{X}^{(1)}(\theta^\alpha) \quad (2)$$

with $\mathbf{X}^{(0)}(\theta^\alpha)$ as the middle surface position vector and $\mathbf{X}^{(1)}(\theta^\alpha)$ as the shell director which both are expressed by the relations

$$\begin{aligned} \mathbf{X}^{(0)}(\theta^\alpha) &= \frac{1}{2} [\mathbf{X}_u(\theta^\alpha) + \mathbf{X}_l(\theta^\alpha)], \\ \mathbf{X}^{(1)}(\theta^\alpha) &= \frac{1}{h} [\mathbf{X}_u(\theta^\alpha) - \mathbf{X}_l(\theta^\alpha)]. \end{aligned}$$

Herein, θ^α , $\alpha = 1, 2$, are middle surface convective coordinates, and θ^3 is the local coordinate in thickness direction. h is the shell thickness.

As presented in more details in Basar and Krätzig (2001), the shell geometry may be described exactly by means of base vectors obtained by partial derivatives of the position vector (2) with respect to the curvilinear coordinates

$$\begin{aligned} \mathbf{G}_\alpha &= \frac{\partial \mathbf{X}(\theta^j)}{\partial \theta^\alpha} = \mathbf{X}^{(0)}(\theta^\delta)_{,\theta^\alpha} + \theta^3 \mathbf{X}^{(1)}(\theta^\delta)_{,\theta^\alpha}, \\ \mathbf{G}_3 &= \frac{\partial \mathbf{X}(\theta^j)}{\partial \theta^3} = \mathbf{X}^{(1)}(\theta^\delta). \end{aligned} \quad (3)$$

As evident, base vector \mathbf{G}_3 is a unit normal middle surface vector. Consequently, the circular cylindrical surface used in the present contribution is defined by means of the following position vector as shown in Figure 2

$$\begin{aligned} \mathbf{X}^{(0)}(\theta^\alpha) \\ = R \cos\left(\frac{\theta^1}{R}\right) \mathbf{e}_1 + R \sin\left(\frac{\theta^1}{R}\right) \mathbf{e}_2 + \theta^2 \mathbf{e}_3, \end{aligned} \quad (4)$$

where R is the radius of the cylinder, and θ^1 and θ^2 are the local coordinates.

3 Kinematics of solid-shell concept

Applying the solid-shell concept according to Hauptmann and Schweizerhof (1998), the displacements may be written in global Cartesian coordinates as

$$\begin{aligned} \mathbf{u}(\theta^j) &= \mathbf{u}^{(0)}(\theta^\alpha) + \theta^3 \mathbf{u}^{(1)}(\theta^\alpha) \\ &+ \frac{1}{2} \left[1 - \left(\frac{2\theta^3}{h} \right)^2 \right] \lambda(\theta^\delta) \mathbf{G}_3, \end{aligned} \quad (5)$$

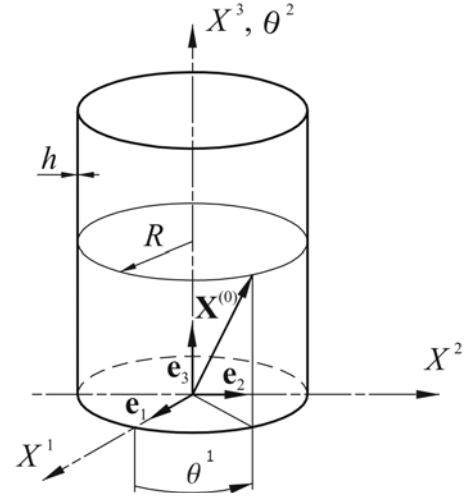


Figure 2: Description of a circular cylindrical surface

where $\mathbf{u}(\theta^j) = u_i(\theta^j) \mathbf{e}_i$ is the displacement vector with the components in directions of the global Cartesian axes. The variables $\mathbf{u}^{(0)}(\theta^\delta)$ and $\mathbf{u}^{(1)}(\theta^\delta)$ are defined by

$$\mathbf{u}^{(0)}(\theta^\delta) = \frac{\mathbf{u}_u + \mathbf{u}_l}{2}, \quad \mathbf{u}^{(1)}(\theta^\delta) = \frac{\mathbf{u}_u - \mathbf{u}_l}{h}, \quad (6)$$

with \mathbf{u}_u and \mathbf{u}_l as the displacement vectors on the upper and lower surfaces, respectively. $\lambda(\theta^\delta)$ is the scalar parameter associated with the quadratic interpolation term in the shell thickness direction according to the hierarchical concept applied.

Adopting the small deformation theory, the strain tensor is defined in the global Cartesian system as

$$\begin{aligned} \varepsilon_{ij} &= \frac{1}{2} \left(\frac{\partial u_i}{\partial X^j} + \frac{\partial u_j}{\partial X^i} \right) \\ &= \frac{1}{2} \left(\frac{\partial u_i}{\partial \theta^p} \frac{\partial \theta^p}{\partial X^j} + \frac{\partial u_j}{\partial \theta^p} \frac{\partial \theta^p}{\partial X^i} \right). \end{aligned} \quad (7)$$

The stress tensor may be obtained by using a generalized Hooke's law

$$\sigma_{ij} = C_{ijkl} \varepsilon_{kl} \quad (8)$$

with C_{ijkl} as the elasticity tensor for the linear isotropic elastic materials. In the global Cartesian system C_{ijkl} is defined as

$$C_{ijkl} = \lambda \delta_{ij} \delta_{kl} + \mu (\delta_{ik} \delta_{jl} + \delta_{il} \delta_{jk}). \quad (9)$$

Herein, μ and λ are Lamé's elastic constants $\mu = \frac{E}{2(1+\nu)}$ and $\lambda = \frac{E\nu}{(1+\nu)(1-2\nu)}$. The components of the surface traction vector may then be expressed by a well known formula

$$t_i = \sigma_{ij}n_j = C_{ijkl}\epsilon_{kl}n_j, \quad (10)$$

where n_j stands for the components of the outward unit normal vector.

4 Governing equations of the MLPG formulation

To derive the governing equations of the proposed computational strategy, we start from the well known equilibrium equations, which in the case of a 3-D static formulation may be written for a domain of volume Ω as follows

$$\sigma_{ij,j} + b_i = 0, \quad \text{in } \Omega, \quad (11)$$

where b_i denotes the body force vector. The domain of Ω is bounded by the surface Γ on which the following boundary conditions are prescribed

$$u_i = \bar{u}_i, \quad \text{on } \Gamma_u, \quad (12)$$

$$t_i = \sigma_{ij}n_j = \bar{t}_i, \quad \text{on } \Gamma_t. \quad (13)$$

Herein, Γ_u is the boundary with prescribed displacements \bar{u}_i , and Γ_t is the boundary with prescribed tractions \bar{t}_i . Now, n_j denotes direction cosines of the outward normal to the boundary surface Γ .

According to the Local Petrov-Galerkin approach described in detail in Atluri (2004), the equilibrium equations (11) may be written in weak form over the local sub-domain Ω_s^I inside Ω as

$$\int_{\Omega_s^I} (\sigma_{ij,j} + b_i) v_{ki} d\Omega - \alpha \int_{\Gamma_{su}^I} (u_i - \bar{u}_i) v_{ki} d\Gamma = 0; \quad I = 1, 2, \dots, N \quad (14)$$

with $v_{ki} = \delta_{ki}v(\theta^j)$, where δ_{ki} is the Kronecker delta and $v(\theta^j)$ denotes an arbitrary test function, as described in Atluri and Zhu (2000). u_i is the trial function describing the displacement field. It is to be noted that the test and trial functions may be chosen from different functional spaces,

and the local sub-domain Ω_s^I could be of any geometric shape. Γ_{su}^I is a part of the boundary $\partial\Omega_s^I$ of the local sub-domain with the prescribed displacements \bar{u}_i , and α denotes a penalty parameter, $\alpha \gg 1$, which is introduced in order to satisfy the geometric boundary conditions.

By employing the divergence theorem and taking $t_i = n_j\sigma_{ij}$ on $\partial\Omega_s^I$ into account, the following Local Symmetric Weak Form (LSWF) is obtained

$$\int_{\partial\Omega_s^I} v_{ki}t_i d\Gamma - \int_{\Omega_s^I} v_{ki,j}\sigma_{ij} d\Omega + \int_{\Omega_s^I} v_{ki}b_i d\Omega - \alpha \int_{\Gamma_{su}^I} v_{ki}(u_i - \bar{u}_i) d\Gamma = 0. \quad (15)$$

The test function is assumed as

$$v(\theta^j) = c_0 + c_1\theta^3 + c_2(\theta^3)^2 \quad (16)$$

with c_0 , c_1 and c_2 as arbitrary chosen real constants. After inserting the test function (16) into (15), the LSWF may be written as

$$\begin{aligned} & c_0 \left[\int_{\Gamma_s^I} t_k d\Gamma + \int_{\Omega_s^I} b_k d\Omega - \alpha \int_{\Gamma_{su}^I} (u_k - \bar{u}_k) d\Gamma \right] \\ & + c_1 \left[\int_{\Gamma_s^I} \theta^3 t_k d\Gamma - \int_{\Omega_s^I} (\theta^3)_{,j} \sigma_{kj} d\Omega + \int_{\Omega_s^I} \theta^3 b_k d\Omega - \alpha \int_{\Gamma_{su}^I} \theta^3 (u_k - \bar{u}_k) d\Gamma \right] \\ & + c_2 \left[\int_{\Gamma_s^I} (\theta^3)^2 t_k d\Gamma - \int_{\Omega_s^I} ((\theta^3)^2)_{,j} \sigma_{kj} d\Omega + \int_{\Omega_s^I} (\theta^3)^2 b_k d\Omega - \alpha \int_{\Gamma_{su}^I} (\theta^3)^2 (u_k - \bar{u}_k) d\Gamma \right] \\ & = 0. \end{aligned} \quad (17)$$

Since relation (17) has to hold for all choices of c_0 , c_1 and c_2 , it yields the following system of

governing equations for the local sub-domain Ω'_s

$$\int_{\Gamma'_s} t_k d\Gamma + \int_{\Omega'_s} b_k d\Omega - \alpha \int_{\Gamma'_{su}} (u_k - \bar{u}_k) d\Gamma = 0,$$

$$\int_{\Gamma'_s} \theta^3 t_k d\Gamma - \int_{\Omega'_s} (\theta^3)_{,j} \sigma_{kj} d\Omega + \int_{\Omega'_s} \theta^3 b_k d\Omega - \alpha \int_{\Gamma'_{su}} \theta^3 (u_k - \bar{u}_k) d\Gamma = 0,$$

$$\int_{\Gamma'_s} (\theta^3)^2 t_k d\Gamma - \int_{\Omega'_s} ((\theta^3)^2)_{,j} \sigma_{kj} d\Omega + \int_{\Omega'_s} (\theta^3)^2 b_k d\Omega - \alpha \int_{\Gamma'_{su}} (\theta^3)^2 (u_k - \bar{u}_k) d\Gamma = 0. \quad (18)$$

In the above equations, the index k takes the values 1, 2 and 3, and thus a set of nine equations for each local sub-domain is derived. However, deformation responses of the shell continuum are described with seven variables through the thickness, including the six displacement components and one additional scalar variable due to the quadratic interpolation through the thickness. It means that only seven equations for each Ω'_s are required for the solution of the boundary value problem. Therefore, three equations represented by the third expression in (18) are summed up in order to form one equation required. Now, the following system of seven governing equations is obtained

$$\int_{\Gamma'_s} t_k d\Gamma + \int_{\Omega'_s} b_k d\Omega - \alpha \int_{\Gamma'_{su}} (u_k - \bar{u}_k) d\Gamma = 0,$$

$$\int_{\Gamma'_s} \theta^3 t_k d\Gamma - \int_{\Omega'_s} (\theta^3)_{,j} \sigma_{kj} d\Omega + \int_{\Omega'_s} \theta^3 b_k d\Omega - \alpha \int_{\Gamma'_{su}} \theta^3 (u_k - \bar{u}_k) d\Gamma = 0,$$

$$\sum_{k=1}^3 \left[\int_{\Gamma'_s} (\theta^3)^2 t_k d\Gamma - \int_{\Omega'_s} ((\theta^3)^2)_{,j} \sigma_{kj} d\Omega \right]$$

$$\left. + \int_{\Omega'_s} (\theta^3)^2 b_k d\Omega - \alpha \int_{\Gamma'_{su}} (\theta^3)^2 (u_k - \bar{u}_k) d\Gamma \right] = 0. \quad (19)$$

5 Discretization of the shell continuum

The continuum is discretized in the convected coordinate system by nodes located on the upper and lower surfaces in the parametric space and is then mapped into the global Cartesian coordinate system, as shown in Figure 3.

Deformation responses of the shell structures are described by the displacement field in the global Cartesian coordinate system (5), which may be written in matrix form as

$$\mathbf{u}(\theta^i) = \mathbf{T}(\theta^\delta) \Psi(\theta^3) \cdot \begin{bmatrix} \mathbf{T}^{-1}(\theta^\delta) & \mathbf{0} & \mathbf{0} \\ \mathbf{0} & \mathbf{T}^{-1}(\theta^\delta) & \mathbf{0} \\ \mathbf{0} & \mathbf{0} & 1 \end{bmatrix} \begin{bmatrix} \mathbf{u}^{(0)}(\theta^\delta) \\ \mathbf{u}^{(1)}(\theta^\delta) \\ \lambda(\theta^\delta) \end{bmatrix}. \quad (20)$$

Herein, the displacement interpolation in the shell thickness direction is described by $\Psi(\theta^3)$ which is given as

$$\Psi(\theta^3) = \begin{bmatrix} 1 & 0 & 0 & \theta^3 & 0 & 0 & 0 \\ 0 & 1 & 0 & 0 & \theta^3 & 0 & 0 \\ 0 & 0 & 1 & 0 & 0 & \theta^3 & \gamma(\theta^3) \end{bmatrix}, \quad (21)$$

where the function $\gamma(\theta^3)$, describing the quadratic interpolation of the transversal displacement component, is defined by the expression

$$\gamma(\theta^3) = \frac{1}{2} \left[1 - \left(\frac{\theta^3}{0.5h} \right)^2 \right]. \quad (22)$$

Furthermore, $\mathbf{T}(\theta^\delta) = \mathbf{J}(\theta^\delta, \theta^3 = 0)$ stands for the transformation matrix from the shell middle surface curvilinear coordinates to the global Cartesian coordinate system, and the Jacobian matrix \mathbf{J} is defined as

$$\mathbf{J} = \begin{bmatrix} \frac{\partial X^1}{\partial \theta^1} & \frac{\partial X^1}{\partial \theta^2} & \frac{\partial X^1}{\partial \theta^3} \\ \frac{\partial X^2}{\partial \theta^1} & \frac{\partial X^2}{\partial \theta^2} & \frac{\partial X^2}{\partial \theta^3} \\ \frac{\partial X^3}{\partial \theta^1} & \frac{\partial X^3}{\partial \theta^2} & \frac{\partial X^3}{\partial \theta^3} \end{bmatrix} = [\mathbf{G}_1 \quad \mathbf{G}_2 \quad \mathbf{G}_3]. \quad (23)$$

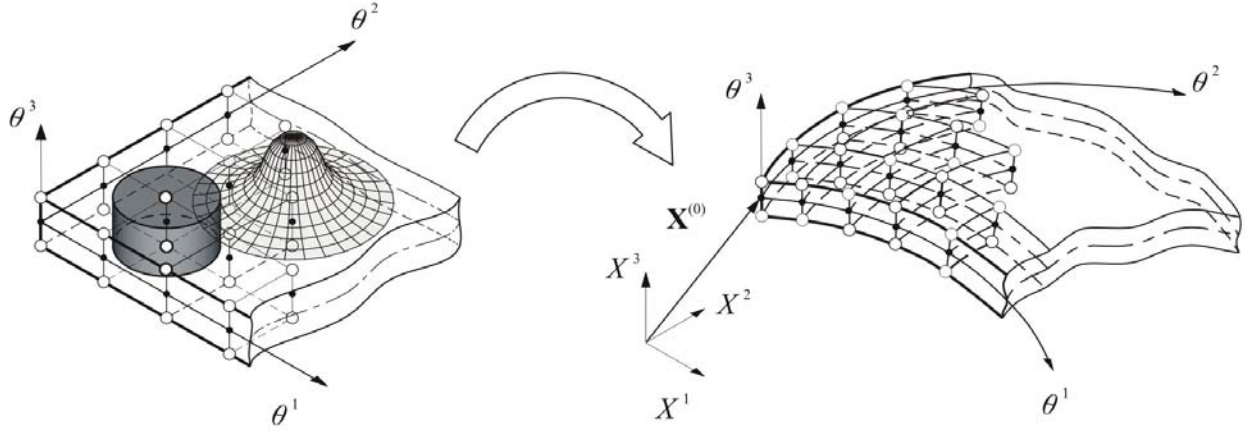


Figure 3: Discretization of shell continuum and mapping from parametric space to Cartesian coordinates

Likewise, the inverse transformation matrix may be expressed as $\mathbf{T}^{-1}(\theta^\delta) = \mathbf{J}^{-1}(\theta^\delta, \theta^3 = 0)$, where \mathbf{J}^{-1} is written in terms of contravariant basis vectors

$$\mathbf{J}^{-1}(\theta^\delta, \theta^3 = 0) = \begin{bmatrix} \mathbf{G}^1 \\ \mathbf{G}^2 \\ \mathbf{G}^3 \end{bmatrix}. \quad (24)$$

As evident from (20), the variables $\mathbf{u}^{(0)}(\theta^\delta)$, $\mathbf{u}^{(1)}(\theta^\delta)$ and $\lambda(\theta^\delta)$ are transformed to convective coordinates due to the interpolation over the thickness which is performed separately from the in-plane interpolation in the θ^1 and θ^2 directions. The in-plane interpolation has been performed by employing the Moving Least Square (MLS) approximation strategy. Thus, the variables $\mathbf{u}^{(0)}(\theta^\delta)$, $\mathbf{u}^{(1)}(\theta^\delta)$ and $\lambda(\theta^\delta)$ may be written in dependence on the nodal values over the domain of influence containing N couples of nodes as

$$\begin{aligned} \mathbf{u}^{(0)}(\theta^\delta) &= \sum_{J=1}^N \phi_J(\theta^\delta) \hat{\mathbf{v}}_J^{(0)}, \\ \mathbf{u}^{(1)}(\theta^\delta) &= \sum_{J=1}^N \phi_J(\theta^\delta) \hat{\mathbf{v}}_J^{(1)}, \\ \lambda(\theta^\delta) &= \sum_{J=1}^N \phi_J(\theta^\delta) \hat{\lambda}_J, \end{aligned} \quad (25)$$

where $\phi_J(\theta^\delta)$ is the in-plane MLS shape function, and the fictitious nodal values are $\hat{\mathbf{v}}_J^{(0)}$, $\hat{\mathbf{v}}_J^{(1)}$ and $\hat{\lambda}_J$. The domain of influence is a region that covers all nodes whose weight functions do not

vanish in the local sub-domain surrounding a current node, as described in Atluri and Zhu (1998). The MLS nodal shape function $\phi_J(\theta^\delta)$ is defined as

$$\phi_J(\theta^\alpha) = \sum_{i=1}^m p_i(\bar{\theta}^\alpha) [\mathbf{A}^{-1}\mathbf{B}]_{iJ} \quad (26)$$

with \mathbf{A} as a momentum matrix of the MLS approximation

$$\mathbf{A} = \sum_{J=1}^N W_J(\theta^\alpha) \mathbf{p}(\bar{\theta}_J^\alpha) \mathbf{p}^T(\bar{\theta}_J^\alpha), \quad (27)$$

and the matrix \mathbf{B} defined as

$$\mathbf{B} = \begin{bmatrix} W_1(\theta^\alpha) \mathbf{p}(\bar{\theta}_1^\alpha) & W_2(\theta^\alpha) \mathbf{p}(\bar{\theta}_2^\alpha) \\ \dots & W_J(\theta^\alpha) \mathbf{p}(\bar{\theta}_J^\alpha) \dots W_N(\theta^\alpha) \mathbf{p}(\bar{\theta}_N^\alpha) \end{bmatrix}. \quad (28)$$

Herein, $\mathbf{p}(\bar{\theta}^\alpha)$ is the complete monomial basis of order m defined in terms of the local normalized coordinates $\bar{\theta}^\alpha$

$$\mathbf{p}^T(\bar{\theta}^\alpha) = [p_1(\bar{\theta}^\alpha) p_2(\bar{\theta}^\alpha) \dots p_j(\bar{\theta}^\alpha) \dots p_m(\bar{\theta}^\alpha)]. \quad (29)$$

The normalized local coordinates of $\bar{\theta}^\alpha = (\theta^\alpha - \theta_0^\alpha)/R_{\max}$ are used in order to avoid a possible ill-conditioning of the momentum matrix \mathbf{A} , similarly as in [Krystl and Belytschko (1995); Raju and Phillips (2003)]. In the proposed formulation, R_{\max} is a distance between a current sample point

θ_0^α and the farthest node in the domain of definition of MLS function. Furthermore, $W_J(\theta^\alpha)$ is the weight function of the MLS approximation associated with node J . In this work, $W_J(\theta^\alpha)$ is chosen as 4th order spline function

$$W_J(\theta^\alpha) = \begin{cases} 1 - 6 \left(\frac{d_J}{r_J}\right)^2 + 8 \left(\frac{d_J}{r_J}\right)^3 - 3 \left(\frac{d_J}{r_J}\right)^4; & 0 \leq d_J \leq r_J \\ 0; & d_J > r_J \end{cases}, \quad (30)$$

where $d_J = |\theta^\alpha - \theta_J^\alpha|$ is the distance between the node J and the current sample point in the parametric space.

By using the MLS approximations (25), the displacement field (20) may now be expressed by the relation

$$\mathbf{u}(\theta^i) = \sum_{J=1}^N \Phi_J(\theta^i) \hat{\mathbf{v}}_J, \quad (31)$$

where $\Phi_J(\theta^i)$ is the 3-D nodal shape function for the node J ; $J = 1, 2, \dots, N$, which has the following form

$$\Phi_J(\theta^i) = \phi_J(\theta^\delta) \mathbf{T}(\theta^\delta) \Psi(\theta^3) \cdot \begin{bmatrix} \mathbf{T}^{-1}(\theta^\delta) & \mathbf{0} & \mathbf{0} \\ \mathbf{0} & \mathbf{T}^{-1}(\theta^\delta) & \mathbf{0} \\ \mathbf{0} & \mathbf{0} & 1 \end{bmatrix}, \quad (32)$$

and $\hat{\mathbf{v}}_J$ is the vector of nodal unknowns

$$\hat{\mathbf{v}}_J^T = \left[\left(\hat{\mathbf{v}}_J^{(0)}\right)^T \quad \left(\hat{\mathbf{v}}_J^{(1)}\right)^T \quad \hat{\lambda}_J \right] \\ = \left[\hat{u}_J^{(0)} \quad \hat{v}_J^{(0)} \quad \hat{w}_J^{(0)} \quad \hat{u}_J^{(1)} \quad \hat{v}_J^{(1)} \quad \hat{w}_J^{(1)} \quad \hat{\lambda}_J \right]. \quad (33)$$

It should be noted that the shape function derived does not possess Kronecker Delta property, which means that $\hat{\mathbf{v}}_J$ are the fictitious nodal values.

The complete 3-D strain tensor may be calculated by using the standard 3-D kinematic differential operator \mathbf{D}_k

$$\boldsymbol{\varepsilon} = \mathbf{D}_k \mathbf{u} = \mathbf{D}_k \sum_{J=1}^N \Phi_J \hat{\mathbf{v}}_J = \sum_{J=1}^N \mathbf{B}_J \hat{\mathbf{v}}_J. \quad (34)$$

Herein, \mathbf{B}_J represents the strain-displacement matrix which in detail is written as

$$\mathbf{B}_J = \mathbf{D}_k \Phi_J = \begin{bmatrix} \phi_{J,\theta^p J_{p1}^{-1}} & 0 & 0 & (\theta^3 \phi_J)_{,\theta^p J_{p1}^{-1}} & 0 \\ 0 & \phi_{J,\theta^p J_{p2}^{-1}} & 0 & 0 & (\theta^3 \phi_J)_{,\theta^p J_{p2}^{-1}} \\ 0 & 0 & \phi_{J,\theta^p J_{p3}^{-1}} & 0 & 0 \\ \phi_{J,\theta^p J_{p2}^{-1}} & \phi_{J,\theta^p J_{p1}^{-1}} & 0 & (\theta^3 \phi_J)_{,\theta^p J_{p2}^{-1}} & (\theta^3 \phi_J)_{,\theta^p J_{p1}^{-1}} \\ 0 & \phi_{J,\theta^p J_{p3}^{-1}} & \phi_{J,\theta^p J_{p2}^{-1}} & 0 & (\theta^3 \phi_J)_{,\theta^p J_{p3}^{-1}} \\ \phi_{J,\theta^p J_{p3}^{-1}} & 0 & \phi_{J,\theta^p J_{p1}^{-1}} & (\theta^3 \phi_J)_{,\theta^p J_{p3}^{-1}} & 0 \\ \dots & \dots & \dots & \dots & \dots \\ 0 & 0 & 0 & (G_{3X} \gamma \phi_J)_{,\theta^p J_{p1}^{-1}} & 0 \\ 0 & 0 & 0 & (G_{3Y} \gamma \phi_J)_{,\theta^p J_{p2}^{-1}} & 0 \\ (\theta^3 \phi_J)_{,\theta^p J_{p3}^{-1}} & 0 & 0 & (G_{3Z} \gamma \phi_J)_{,\theta^p J_{p3}^{-1}} & 0 \\ 0 & 0 & 0 & (G_{3X} \gamma \phi_J)_{,\theta^p J_{p2}^{-1}} + (G_{3Y} \gamma \phi_J)_{,\theta^p J_{p1}^{-1}} & 0 \\ (\theta^3 \phi_J)_{,\theta^p J_{p2}^{-1}} & (G_{3Y} \gamma \phi_J)_{,\theta^p J_{p3}^{-1}} + (G_{3Z} \gamma \phi_J)_{,\theta^p J_{p2}^{-1}} & 0 & 0 & 0 \\ (\theta^3 \phi_J)_{,\theta^p J_{p1}^{-1}} & (G_{3X} \gamma \phi_J)_{,\theta^p J_{p3}^{-1}} + (G_{3Z} \gamma \phi_J)_{,\theta^p J_{p1}^{-1}} & 0 & 0 & 0 \end{bmatrix}, \quad (35)$$

where $J_{pi}^{-1} = \partial \theta^p / \partial X^i$ denote the terms of the inverse Jacobian matrix defined in (24). Values G_{3X} , G_{3Y} and G_{3Z} stand for the components of the covariant base vector \mathbf{G}_3 in the global Cartesian system. The stress tensor is obtained by employing a generalized Hooke's law

$$\boldsymbol{\sigma} = \mathbf{D} \boldsymbol{\varepsilon} = \mathbf{D} \sum_{J=1}^N \mathbf{B}_J \hat{\mathbf{v}}_J = \sum_{J=1}^N \mathbf{D} \mathbf{B}_J \hat{\mathbf{v}}_J \quad (36)$$

with \mathbf{D} as the 3-D elasticity matrix. The surface traction vector may also be expressed in vector form by the relation

$$\mathbf{t} = \mathbf{N} \boldsymbol{\sigma} = \mathbf{N} \sum_{J=1}^N \mathbf{D} \mathbf{B}_J \hat{\mathbf{v}}_J = \sum_{J=1}^N \mathbf{N} \mathbf{D} \mathbf{B}_J \hat{\mathbf{v}}_J, \quad (37)$$

where \mathbf{N} represents the following matrix containing the components of the outward unit normal vector $\mathbf{n} = n_i \mathbf{e}_i$ on $\partial \Omega_s^I$

$$\mathbf{N} = \begin{bmatrix} n_1 & 0 & 0 & n_2 & 0 & n_3 \\ 0 & n_2 & 0 & n_1 & n_3 & 0 \\ 0 & 0 & n_3 & 0 & n_2 & n_1 \end{bmatrix}. \quad (38)$$

By means of expressions (31), (34), (36) and (37), and after introducing the boundary conditions (12) and (13), the governing equations (19) for a couple of nodes I may be transformed into

the following discretized set of linear equations

$$\sum_{J=1}^N \left[\int_{L_s^I} \mathbf{NDB}_J d\Gamma + \int_{\Gamma_{su}^I} \mathbf{NDB}_J d\Gamma - \alpha \int_{\Gamma_{st}^I} \Phi_J d\Gamma \right] \hat{\mathbf{v}}_J = - \int_{\Omega_s^I} \mathbf{b} d\Omega - \int_{\Gamma_{st}^I} \bar{\mathbf{t}} d\Gamma - \alpha \int_{\Gamma_{su}^I} \bar{\mathbf{u}} d\Gamma, \quad (39)$$

$$\sum_{J=1}^N \left[\int_{L_s^I} \theta^3 \mathbf{NDB}_J d\Gamma + \int_{\Gamma_{su}^I} \theta^3 \mathbf{NDB}_J d\Gamma - \int_{\Omega_s^I} \nabla \mathbf{v}_1^T \mathbf{DB}_J d\Omega - \alpha \int_{\Gamma_{su}^I} \theta^3 \Phi_J d\Gamma \right] = - \int_{\Omega_s^I} \theta^3 \mathbf{b} d\Omega - \int_{\Gamma_{st}^I} \theta^3 \bar{\mathbf{t}} d\Gamma - \alpha \int_{\Gamma_{su}^I} \theta^3 \bar{\mathbf{u}} d\Gamma, \quad (40)$$

$$\sum_{J=1}^N \left[\int_{L_s^I} \mathbf{v}_2^T \mathbf{NDB}_J d\Gamma + \int_{\Gamma_{su}^I} \mathbf{v}_2^T \mathbf{NDB}_J d\Gamma - \int_{\Omega_s^I} \nabla \mathbf{v}_2^T \mathbf{DB}_J d\Omega - \alpha \int_{\Gamma_{su}^I} \mathbf{v}_2^T \Phi_J d\Gamma \right] \hat{\mathbf{v}}_J = - \int_{\Omega_s^I} \mathbf{v}_2^T \mathbf{b} d\Omega - \int_{\Gamma_{st}^I} \mathbf{v}_2^T \bar{\mathbf{t}} d\Gamma - \alpha \int_{\Gamma_{su}^I} \mathbf{v}_2^T \bar{\mathbf{u}} d\Gamma \quad (41)$$

with

$$\mathbf{v}_2^T = [(\theta^3)^2 \quad (\theta^3)^2 \quad (\theta^3)^2], \quad (42)$$

$$\nabla \mathbf{v}_1^T = \begin{bmatrix} \theta^3_{,1} & 0 & 0 & \theta^3_{,2} & 0 & \theta^3_{,3} \\ 0 & \theta^3_{,2} & 0 & \theta^3_{,1} & \theta^3_{,3} & 0 \\ 0 & 0 & \theta^3_{,3} & 0 & \theta^3_{,2} & \theta^3_{,1} \end{bmatrix}, \quad (43)$$

$$\nabla \mathbf{v}_2^T = \begin{bmatrix} (\theta^3)^2_{,1} & (\theta^3)^2_{,2} & (\theta^3)^2_{,3} & (\theta^3)^2_{,2} + (\theta^3)^2_{,1} & & \\ \dots & (\theta^3)^2_{,3} + (\theta^3)^2_{,2} & (\theta^3)^2_{,3} + (\theta^3)^2_{,1} & & & \end{bmatrix}. \quad (44)$$

In the expressions (39)-(41), the local boundary has been decomposed into three parts, i.e. $\partial\Omega_s^I = L_s^I \cup \Gamma_{st}^I \cup \Gamma_{su}^I$. Thereby, L_s^I is the part of $\partial\Omega_s^I$ that is completely inside Ω , while Γ_{st}^I and Γ_{su}^I are parts of $\partial\Omega_s^I$ with the prescribed natural and essential boundary conditions, respectively. N is the total number of couples of nodes corresponding to the domain of influence. Body forces are usually neglected in engineering computations, and therefore, all domain integrals involving the body force vector \mathbf{b} can be eliminated. Herein, integration is performed in the curvilinear coordinates over the local sub-domain, where the volume element may be expressed in terms of the base vectors describing the shell geometry considered, as

$$d\Omega = (\mathbf{G}_1 \times \mathbf{G}_2) \mathbf{G}_3 d\theta^1 d\theta^2 d\theta^3. \quad (45)$$

In addition, the surface element $d\Gamma$ depends on the shape of the local sub-domain boundary surface $\partial\Omega_s$.

Now, for each local sub-domain a set of $7N$ equations with equal number of unknowns has to be evaluated for the domain of influence with N couples of nodes. However, the parameter $\hat{\lambda}$ can be eliminated on the level of the domain of influence by employing static condensation described in Sorić Li, Jarak and Atluri (2004), which yields a set of equations with only fictitious nodal displacement components as unknowns. Global equations on the structural level are derived by using a well-known numerical assemblage procedure.

6 Numerical examples

In the following, deformation responses of cylindrical shells are considered as numerical examples. For facilitation, shells are discretized by uniform grids, and the cylindrical shape of any local sub-domain is maintained. In order to satisfy the essential boundary conditions, the well-known penalty method is applied. It has been found that satisfactory results are obtained if the values of the penalty parameter are between 10^5 and 10^{12} . Here, the penalty parameter of $\alpha = 10^9$ is used in all examples.

6.1 Scordelis-Lo shell roof

As first example, the Scordelis-Lo shell roof is considered, as shown in Figure 4. This is a well-known standard benchmark for the analysis of thin shells. Material data are Young’s modulus $E = 30000 \text{ N/mm}^2$ and Poisson’s ratio $\nu = 0.0$. The radius and length of the roof are $R = 3000 \text{ mm}$ and $L = 6000 \text{ mm}$, respectively, and the radius to thickness ratio is $R/h = 100$. The shell is subjected to the uniform vertical load of $q = 0.00625 \text{ N/mm}^2$. It is assumed that the two longitudinal edges are free and the two circular edges are supported by rigid diaphragms. Owing to symmetry, only one quarter of the shell is discretized by a uniform grid.

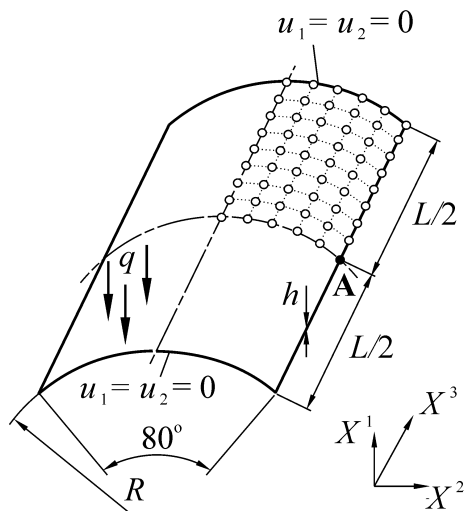


Figure 4: Geometry and discretization of the Scordelis-Lo roof

The convergence rate of the vertical displacement at the middle surface point A normalized by the analytical value from Scordelis and Lo (1969) is presented in Figure 5 for different MLS basis functions.

The results display that the convergence rate increases with increasing order of the MLS basis functions. They also demonstrate that the shear locking effect is minimized by using the 5th and 6th order basis functions. The deformed shape of one quarter of the structure is presented in Figure 6.

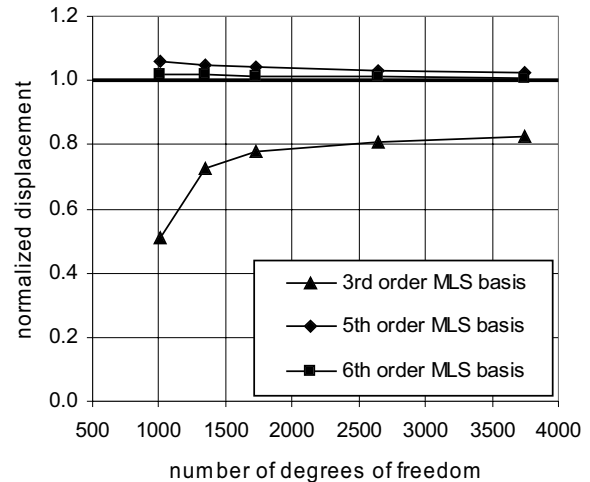


Figure 5: Convergence rate of the vertical displacement at the middle surface point A

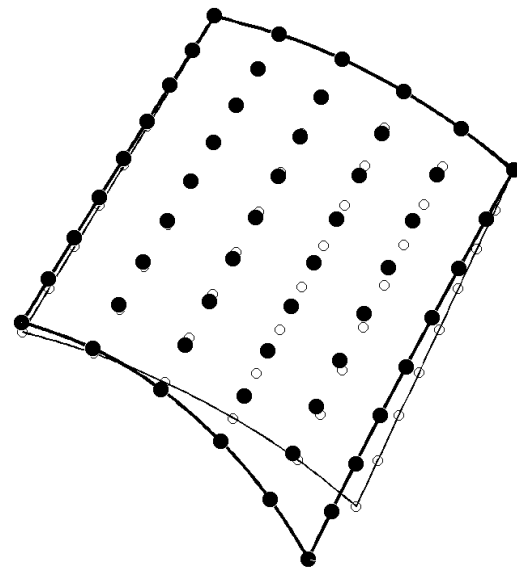


Figure 6: Deformed shape of one quarter of the Scordelis-Lo roof

6.2 Cylindrical shell subjected to uniform line load

A horizontal cylindrical shell shown in Figure 7 is analyzed as second example. The shell is subjected to uniform line load of $q = 1 \text{ N/mm}$ along the upper and the lower generatrix. The shell thickness is $h = 0.9 \text{ mm}$ with the radius to thickness ratio of $R/h = 100$ and the length of the cylinder is $L = 150 \text{ mm}$. The material data are

Young's modulus $E = 210000 \text{ N/mm}^2$ and Poisson's ratio $\nu = 0.3$. Due to symmetry, only one octant of the shell is discretized by a uniform grid. The convergence rate of the vertical displacement

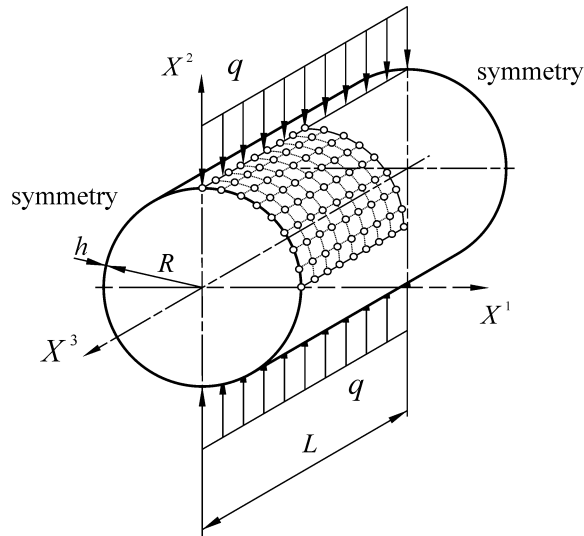


Figure 7: Geometry and discretization of a cylindrical shell subjected to line load

under line load at the central point of the middle surface is again displayed for different MLS basis functions in Figure 8. The results are normalized by the analytical solution from Timoshenko and Voinowsky-Krieger (1985). As evident, the convergence is here achieved by using the 5th order basis function. In Figure 9, the results are compared with the finite element solutions obtained by parabolic 3-D brick-type elements of program package NASTRAN. Satisfactory agreement between the finite element solutions and the results obtained by the present approach is achieved, and a good convergence rate of the meshless formulation is demonstrated.

6.3 Pinched cylinder

A thin cylinder pinched by two radial forces $P = 1\text{N}$ in the middle of the structure and bounded by two rigid diaphragms is analyzed as final example. Geometry and discretization of one octant of the shell are presented in Figure 10. Young's modulus of the material is $E = 3 \times 10^6 \text{ N/mm}^2$ and Poisson's ratio $\nu = 0.3$. The radius to thickness ratio is $R/h = 100$ and the shell thickness is

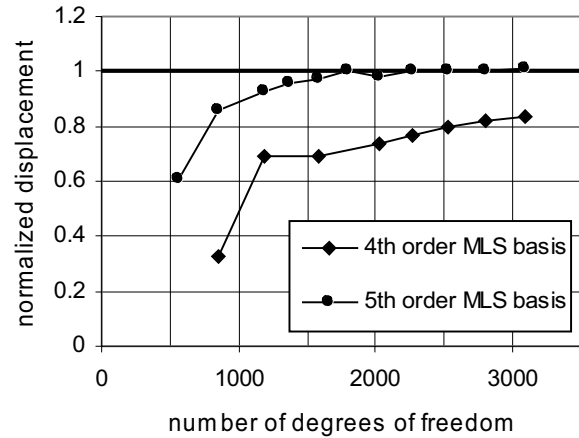


Figure 8: Convergence of the vertical displacement under line load at the middle surface central point

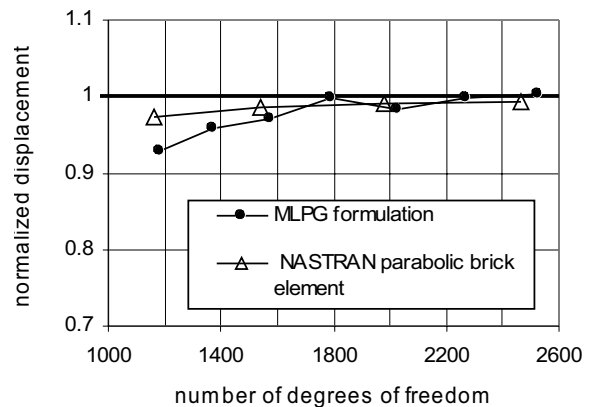


Figure 9: Convergence rate in comparison with the finite element solution

$h = 3 \text{ mm}$. The length of the shell is $L = 600 \text{ mm}$.

The convergence is studied again. The normalized vertical displacement under the point load versus the number of nodal unknowns is plotted in Figure 11.

Normalization has been performed by using the exact solution from Timoshenko and Voinowsky-Krieger (1985). Like in the previous example, the convergence rate increases with increasing order of the MLS basis, which is connected with increasing order of the displacement shape functions. However, due to the pinch loading, the cylinder exhibits larger locking behaviour then it

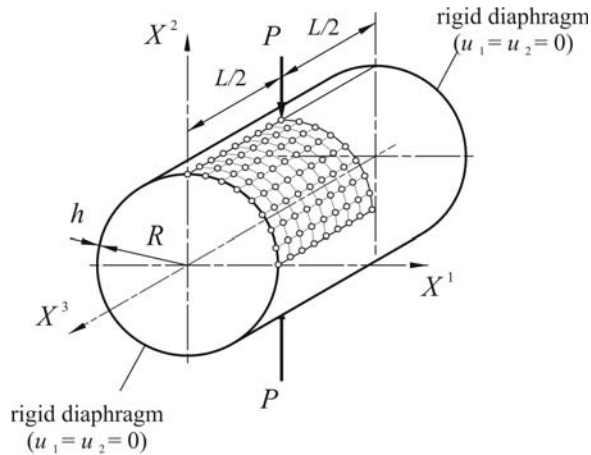


Figure 10: Geometry and discretization of a pinched cylinder

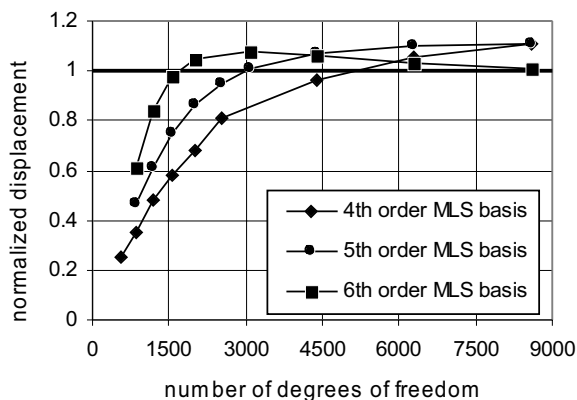


Figure 11: Convergence of the vertical displacement under point load

is observed in the previous examples. Therefore, the 6th order MLS basis is required to achieve the convergence.

7 Conclusion

A meshless formulation based on the Local Petrov-Galerkin approach has been proposed for the analysis of shell structures. The kinematics of a 3-D solid is applied, allowing the use of complete 3-D constitutive equations. The exact shell geometry can be performed. Furthermore, this numerical approach requires no elements or background cells in either interpolation or integration, and it is therefore a truly meshless method.

The local symmetric weak form of equilibrium

equations is derived over the cylindrical local sub-domain, surrounding each couple of nodes located on the upper and lower surfaces. Discretization is performed in the convected coordinate system in the parametric space, and then mapped into the global Cartesian coordinates where arbitrary shell geometries may be described. The nodal unknown variables are fictitious displacement components. Discretization in the in-plane directions is performed by employing the MLS approximation, while simple polynomial interpolations are used for the displacement distribution in thickness direction. Thickness locking is eliminated by using hierarchical quadratic approximation for the transversal displacements over the thickness. The shear locking phenomena in case of thin structures and the sensitivity to rigid body motion due to the exact geometry description are minimized by applying a sufficiently high order of the basis function in the MLS approximation. By properly choice of the weight function support, good convergence rates are achieved as illustrated by several numerical examples.

It should be noted that the present meshless computation is time consuming due to the complex MLS interpolation function. Therefore, a more efficient interpolation function having Kronecker Delta property should be used in further study. By using the new interpolation, geometric boundary conditions could be satisfied exactly, which would also contribute to accuracy of the proposed meshless approach. In addition, other remedies for elimination of shear locking effect, like a mixed meshless approach, are desirable. In order to fully eliminate sensitivity to rigid body motion due to the exact shell geometry description, an isoparametric-like formulation should be considered.

Acknowledgement: The authors like to express their gratitude to the Alexander von Humboldt Foundation from Germany and the Ministry of Science Education and Sport of the Republic of Croatia for financial support.

References

- Atluri, S.N.** (2004): The Meshless Method (MLPG) for Domain & BIE Discretization, Tech Science Press, Forsyth.
- Atluri, S.N.; Zhu, T.** (1998): A new Meshless Local Petrov-Galerkin (MLPG) approach in computational mechanics, *Computational Mechanics*, vol. 22, pp. 117-127.
- Atluri, S.N.; Zhu, T.-L.** (2000): The Meshless Local Petrov-Galerkin (MLPG) approach for solving problems in elasto-statics, *Computational Mechanics*, vol. 25, pp. 169-179.
- Basar, Y.; Krätzig, W.B.** (2001): Theory of Shell Structures, VDI Verlag, Düsseldorf.
- Chen, J-S.; Wang, D.** (2006): A constrained reproducing kernel particle formulation for shear deformable shell in Cartesian coordinates, *Int. J. Numer. Mech. Engng.*, vol. 68, pp. 151-172.
- Hauptmann, R.; Schweizerhof, K.** (1998): A systematic development of solid-shell element formulations for linear and non-linear analyses employing only displacement degrees of freedom, *Int. J. Numer. Meth. Engng.*, vol. 42, pp. 49-69.
- Kim, N.H.; Choi, K.K.; Chen, J-S; Botkin, M.** (2002): Meshfree analysis and design sensitivity analysis for shell structures, *Int. J. Numer. Meth. Engng.*, vol. 53, pp. 2087-2116.
- Klinkel, S.; Gruttmann, F.; Wagner, W.** (2006): A robust non-linear solid shell element based on a mixed variational formulation, *Comput. Methods Appl. Mech. Engng.*, vol. 195, pp. 179-201.
- Krystl, P.; Belytschko T.** (1996): Analysis of thin shells by element-free Galerkin method, *Int. J. Solids Structures*, vol. 33, pp. 3057-3080.
- Krystl, P.; Belytschko, T.** (1995): Analysis of thin plates by the element-free Galerkin method, *Computational Mechanics*, vol. 17, pp. 26-35.
- Li, Q.; Sorić J.; Jarak, T.; Atluri, S.N.** (2005): A locking-free meshless local Petrov-Galerkin formulation for thick and thin plates, *Journal of Computational Physics*, vol. 208, pp. 116-133.
- Liu, G.R.** (2003): Mesh Free Methods: Moving beyond the Finite Element Method, CRC Press, Boca Raton.
- Liu, W.-K.; Li, S.; Belytschko, T.** (1997): Moving least-square reproducing kernel methods (I) Methodology and convergence, *Comput. Methods Appl. Mech. Engng.*, vol. 143, pp. 113-154.
- Noguchi, H.; Kawashima, T., Miyamura, T.** (2000): Element free analyses of shell and spatial structures, *Int. J. Numer. Math. Engng.*, vol. 47, pp. 1215-1240.
- Rabczuk, T.; Areias, P.** (2006): A Meshfree Thin Shell for Arbitrary Evolving Cracks Based on An Extrinsic Basis, *CMES: Computer Modeling in Engineering & Sciences*, vol. 16, no. 2, pp. 115-130.
- Raju, I.S.; Phillips, D.R.** (2003): Further developments in the MLPG Method for beam problems, *CMES: Computer Modeling in Engineering & Sciences*, vol. 4, no. 1, pp. 141-159.
- Scordelis, A.C.; Lo, K.S.** (1969): Computer analysis of cylindrical shells, *Journal of the American Concrete Institute*, vol. 66, pp. 539-561.
- Sladek, J.; Sladek, V.; Wen, P.H.; Aliabadi, M.H.** (2006): Meshless Local Petrov-Galerkin (MLPG) Method for Shear Deformable Shells Analysis, *CMES: Computer Modeling in Engineering & Sciences*, vol. 6, no. 2, pp. 103-117
- Sorić J.; Li, Q.; Jarak, T.; Atluri, S.N.** (2004): Meshless Local Petrov-Galerkin (MLPG) formulation for analysis of thick plates, *CMES: Computer Modeling in Engineering & Sciences*, vol. 6, no. 4, pp. 349-357.
- Tan, X.G.; Vu-Quoc, L.** (2005): Optimal solid shell element for large deformable composite structures with piezoelectric layers and active vibration control, *Int. J. Numer. Mech. Engng.*, vol. 64, pp. 1981-2013.
- Timoshenko, S.; Voinowsky-Krieger, S.** (1985): Theory of Plates and Shells, McGraw-Hill, London.